





Extraction Methods for Small-Scale Features on a Large Scale: Investigating Object-Oriented Cart Decision Tree for Gravel Information Extraction

Yuxin Chen , Weilai Zhang , Jiajia Yang , Yuanyuan Xu , Qian Yuan , Wuxue Cheng , and Li Peng 

Abstract—This study employs the object-oriented Cart (Classification and Regression Trees) decision tree methodology to delineate contiguous gravel areas within Zamu town. The primary objective is to devise a technique capable of efficiently identifying small-scale features on a macroscopic scale. Given the pervasive and uninterrupted distribution of background elements like forests, snow, and water in the designated study zone, the removal of these features can significantly bolster the precision of target feature extraction. The elimination of these background elements predominantly hinges on the application of index thresholds. Specifically, the Normalized Difference Vegetation Index (NDVI), Normalized Difference Water Index (NDWI), and Normalized Difference Snow Index (NDSI) are employed to filter out these nontarget features. Following this, Google HD historical imagery is integrated with Sentinel-2 data to facilitate the object-oriented Cart decision tree-based feature extraction. Our findings underscore that both NDVI and NDWI are pivotal in eradicating forest backgrounds. For differentiating snow-covered terrains, the NDVI and NDSI indices prove particularly vital. The identification of water bodies necessitates the synergistic use of all three indices. Notably, the Cart decision tree approach, grounded in the “cull, filter, classify, and merge” philosophy, showcases superior classification accuracy relative to other supervised classification techniques. In the realm of decision tree rule formulation, spectral features dominate, constituting 47.6% of the land class classification. Concurrently, texture features are instrumental, accounting for 38.1%. These texture features exhibit an enhanced discriminatory capacity, whereas the incorporation of diverse indices offers limited incremental value. Pertinently, within the suite of features conducive to gravel extraction, both the Blue band and gray-level co-occurrence matrix entropy emerge as particularly efficacious.

Index Terms—Feature extraction, image classification, image segmentation.

I. INTRODUCTION

GRAVEL is pivotal in a myriad of applications, including environmental, military, marine as well as mining, agriculture, and more [1], [2], [3], [4]. It stands as an indispensable material in realms such as construction, flood control, hydraulic engineering, and agriculture [5], [6], [7]. The judicious extraction and utilization of gravel not only underpin infrastructure but also maintain an ecological equilibrium in aquatic environments. They further catalyze agricultural and industrial growth and hold significance in ecological restoration and landscape design. A precise identification and delineation of gravel sites bolster its pragmatic application [8], [9].

Historically, the majority of gravel extraction research has been riveted on proximal river regions [10], predominantly leveraging measured data. Such studies invariably spotlight gravel resources in riverbeds and along riverbanks, given their propensity for gravel accumulation [11], [12], [13]. The conventional approach involves harnessing various measurement data coupled with geological surveys to ascertain gravel’s distribution and characteristics, thereby optimizing its extraction. However, this modus operandi is not without its constraints. It often narrows its lens to specific geographical terrains, sidelining a holistic view of gravel distribution across expansive regions. Moreover, an overreliance on measured data grapples with challenges like sparse sampling points, prohibitive costs, and extended timeframes.

In light of these challenges, the ascendancy of remote sensing technology in gravel extraction has been a game-changer. This technology, with its expansive coverage, accessibility, and time efficiency, offers a panacea to traditional limitations [14], [15]. Through high-resolution imagery from satellites or aerial cameras, researchers can discern gravel distribution patterns and even proffer estimates on gravel volume. Such insights not only illuminate gravel distribution over vast terrains but also inform strategic planning and resource stewardship [16], [17].

The advent of remote sensing technology has revolutionized gravel extraction, facilitating swift and precise identification of gravel sites and tracking their evolutionary trends. This is invaluable for long-term strategic planning and resource governance. In recent times, the formidable data processing prowess of the

Manuscript received 3 June 2023; revised 13 August 2023 and 19 October 2023; accepted 23 October 2023. Date of publication 3 November 2023; date of current version 23 November 2023. This work was supported in part by the Humanities and Social Sciences, Ministry of Education of The People’s Republic of China under Grant 18YJC850004, and in part by the National Natural Science Foundation of China under Grant 32060370. (Corresponding author: Wuxue Cheng.)

Yuxin Chen, Weilai Zhang, Jiajia Yang, and Yuanyuan Xu are with the Faculty Geography Resources Sciences, Sichuan Normal University, Chengdu 610101, China (e-mail: 20211101051@stu.sicnu.edu.cn; 20221101012@stu.sicnu.edu.cn; 20211101056@stu.sicnu.edu.cn; 20211101059@stu.sicnu.edu.cn).

Wuxue Cheng and Li Peng are with the Faculty Geography Resources Sciences, Sichuan Normal University, Chengdu 610101, China, and also with the Key Laboratory of Land Resources Evaluation and Monitoring in Southwest China, Sichuan Normal University, Chengdu 610066, China (e-mail: cw714826@sicnu.edu.cn; pengli@imde.ac.cn).

Qian Yuan is with the School of Surveying and Engineering Information, Henan Polytechnic University (HPU), Jiaozuo 454003, China (e-mail: hpuyqian@163.com).

Digital Object Identifier 10.1109/JSTARS.2023.3329258

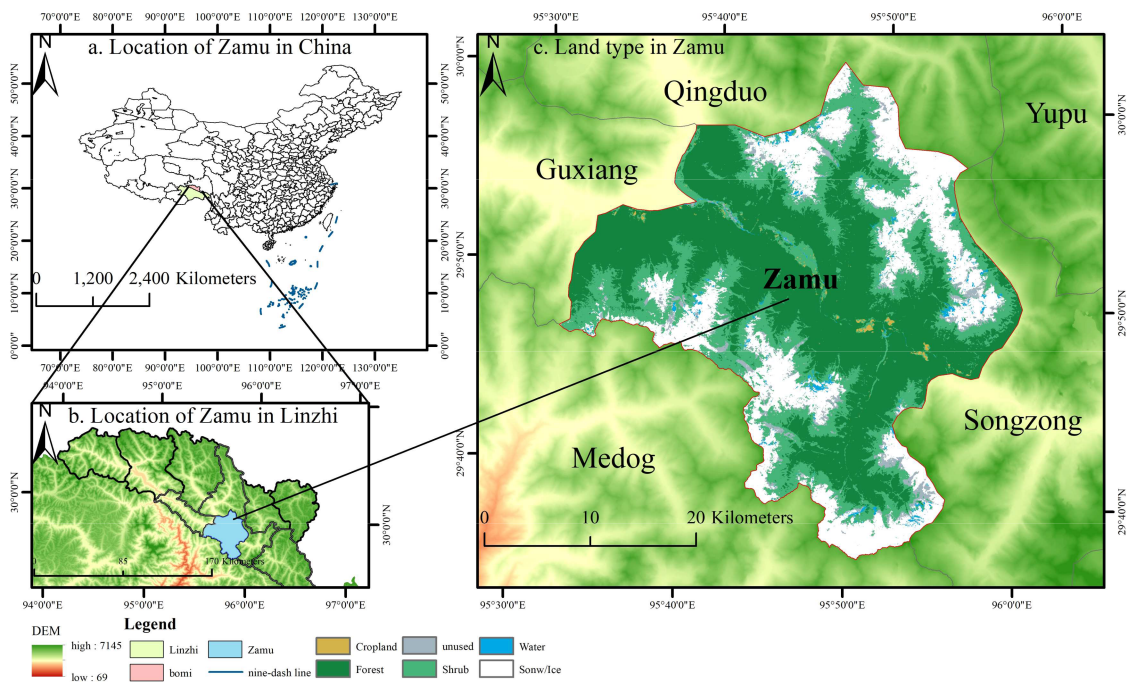


Fig. 1. Location map of Zamu.

Google Earth Engine (GEE) has captivated the research community [18], [19], [20]. This platform not only simplifies remote sensing data processing but also heralds novel avenues for gravel analytics. GEE’s unparalleled efficacy equips researchers with a potent tool, ushering in innovative paradigms for probing gravel distribution and its evolution [15], [18].

Gravel extraction and classification through remote sensing imagery have matured significantly. These techniques typically harness spectral and texture data from multispectral and hyperspectral images. Enhanced spatial resolution has lessened the challenges posed by mixed image elements. Object-oriented target extraction has taken center stage in research, segmenting spectral, and texture data between adjacent image elements to delineate different regions and classify targets.

For instance, Masoumi et al. [21] utilized spectral and texture features from ASTER data, applying random forest (RF) and principal component analysis algorithms to classify rocks, achieving a classification accuracy of 77.21%. Li et al. [22] focused on rock depth features, leveraging a deep convolutional neural network migration method on high-resolution data, which improved large-scale image element analysis. Grebby et al. [23] combined spectral and topographic data with an object-oriented classifier, outperforming pixel-based classification algorithms. Despite these advancements, a gap remains in methods that extract small-scale features over expansive areas, particularly those integrating Google HD images and Sentinel data via the GEE platform. In this study, we employ Google HD images, combined with a priori knowledge, and use thresholding to eliminate background values, extracting gravels through an object-oriented Cart (Classification and Regression Trees) approach.

Cart is a decision tree algorithm introduced by Leo Breiman in 1984. It is renowned in machine learning and data mining for classification and regression tasks. The algorithm crafts a binary

tree where each internal node denotes a decision based on a feature, and each leaf node signifies a class label or predicted value. Cart’s application in remote sensing spans feature classification, land use/land cover change detection, and urban growth analysis. For example, Bar et al. compared Cart, RFs, and support vector machines (SVM) for identifying forest fires using Landsat 8 and Sentinel-2 Optical Satellite Imagery. Cart outperformed SVM and showcased the benefits of merging unsupervised and supervised algorithms on GEE [24]; Sang et al [25] employed Landsat imagery and the Cart method to extract land use data for Tianjin city, introducing a land use intensity analysis approach. Our study leverages supervised classification techniques such as KNN, RF, NB, and SVM on the GEE platform. We juxtapose these methods against the object-oriented Cart decision tree classification approach to analyze gravel distribution. This comparative analysis seeks to pinpoint the optimal method, offering insights for related research domains.

II. STUDY AREA AND DATASETS

A. Study Area

Zamu town, nestled in Bomi County within Linzhi City of the Tibet Autonomous Region, is geographically positioned at $29^{\circ}14'47''\text{N}$ and $95^{\circ}26'25''\text{E}$. This can be seen in Fig. 1. This locale is ensconced on the northern foothills of the eastern Himalayas, boasting an average elevation of 2720 meters. Its landscape is predominantly an alluvial plain, influenced by a plateau temperate semi-humid monsoon climate. While the region enjoys generous rainfall, sunshine is comparatively sparse, with an extended frost-free duration. Yearly average temperature hovers around 8.5°C , with an annual precipitation of approximately 876.9 mm [26], [27].

A breakdown of the land distribution reveals that cultivated land comprises a mere 0.3% of the total expanse. Vegetation, predominantly forests interspersed with shrubs and grasslands, blankets 71% of the area. Water bodies account for 1.1%, snow and ice cover about 23%, and unused land makes up roughly 3.5%.

Zamu town is not just a geographical landmark; it's the administrative heart of Bomi County and a pivotal transportation nexus. Despite its bustling population and economic vibrancy, intricate topography poses challenges to expansive land resource utilization. Animal husbandry and tourism anchor the town's economy, reflecting its unique blend of natural and cultural offerings. Within the broader canvas of the Tibetan Plateau, Zamu town's distinct climatic and topographical attributes endow it with a special natural status. Gravels here underpin agricultural endeavors, water retention, and conservation of soil and water. Consequently, delving into gravel extraction in Zamu can shed light on regional evolution and shifts in land utilization [28].

B. Datasets

1) *Sentinel-2 Data Set*: Part of the Earth observation program initiated by the European Space Agency, the Sentinel-2 data set offers high-resolution remote sensing images for global land cover and land use monitoring. This data set includes a series of satellites equipped with the multispectral imager sensor, capturing images in 13 bands with spatial resolutions between 10 and 60 m. These bands span a broad spectral range from visible to near-infrared wavelengths. For this study, we sourced Sentinel-2 data from the "Sentinel-2 Surface Reflectance" dataset available on GEE here. Our focus was on the dataset spanning the entire year of 2020, which incorporates seven bands (1, 2, 3, 4, 8, 11, and 12). Images in this dataset have undergone processes such as radiometric calibration, atmospheric correction, and surface reflectance conversion to ensure accurate surface representation.

2) *Google HD Images*: We sourced Google HD images from Google Earth Pro, specifically selecting historical images of Zamu town dated January 13, 2020. SASPlanet software facilitated the download, aiding in the retrieval and management of this high-resolution imagery.

3) *Land cover dataset*: Originating from the research paper "30 m annual land cover and its dynamics in China from 1990 to 2019" by Prof. Jie Yang and Prof. Xin Huang, this dataset now extends from 1985 to 2020 with a 30-m spatial resolution. For our study, we chose the 2020 data for analysis [29].

4) *Data preprocessing*: Several critical steps define the data preprocessing phase. Initially, we fused the monthly red, green, and blue bands of Google HD images with bands 1, 4, 11, and 12 of the Sentinel-2 dataset. This fusion aims to generate a composite image of higher resolution, merging spatial details from Google HD images with spectral information from Sentinel-2 data. Such an integrated image offers a richer representation of the study area. Subsequently, we calculated various indices using the maximum synthesis approach. Indices like the Normalized Difference Vegetation Index (NDVI), Normalized Difference Water Index (NDWI), and Normalized Difference Snow Index (NDSI) were derived from the fused imagery. These indices are

instrumental in evaluating vegetation coverage, water bodies, and snow presence. Analyzing these indices provides insights into the distribution and characteristics of these features in the study area [30], [31], [32].

Through these data preprocessing steps, our objective is to bolster the imagery's quality and informational depth, facilitating a precise and comprehensive analysis of gravel extraction in the region.

III. METHODOLOGY

A. Brief Description

Both supervised and unsupervised classifications stand as the predominant methods for image classification in remote sensing [33], [34], [35], [36], [37]. Yet, they demand high image quality and often fall short when extracting features in small-scale and intricate scenes [38], [39]. In contrast, the object-oriented classification method categorizes each object based on its inherent features. By allowing the integration of multiple attributes, it bolsters the reliability and stability of the classification. This method excels in preserving spatial information, making it apt for extracting diminutive features from high-resolution images [40]. Consequently, object-oriented classification techniques have garnered significant interest in recent times [41], [42]. Diverging from traditional methods that pigeonhole individual pixels, the object-oriented approach delves into the spatial interplay between pixels. This nuanced perspective facilitates a more precise and granular analysis. By amalgamating pixels into coherent objects, such as edifices, thoroughfares, or vegetation clusters, it offers a holistic grasp of the scene's makeup and architecture. This method weighs the contextual data, morphological traits, and spectral properties of objects, leading to enhanced classification precision and a superior depiction of intricate features [43], [44].

In our study, we champion a novel technique to extract gravel from contiguous zones using the object-oriented Cart method. This strategy zeroes in on the macroscopic extraction of microscopic features, adhering to the "cull, filter, classify, and merge" paradigm, as illustrated in Fig. 2.

B. Rejecting Background Features

High-resolution image data is imperative for gravel extraction. Yet, the computational demands and image quality prerequisites of object-oriented feature extraction methods often confine their use to smaller-scale images [19]. Given this constraint, it becomes essential to eliminate prominent background features in the study area before embarking on object-oriented target extraction. In Zamu town, significant tracts are blanketed by snow, forests, and water. These elements, deemed as background features, need removal to streamline object-oriented processing.

To achieve this, our study employs the index threshold method, pinpointing specific indices for scrutiny. Notably, we focus on the NDVI, NDWI, and NDSI as pertinent indices. We then undertake a month-by-month synthesis of these indices to ascertain their annual peak values. This strategy facilitates the recognition and evaluation of key features such as vegetation,

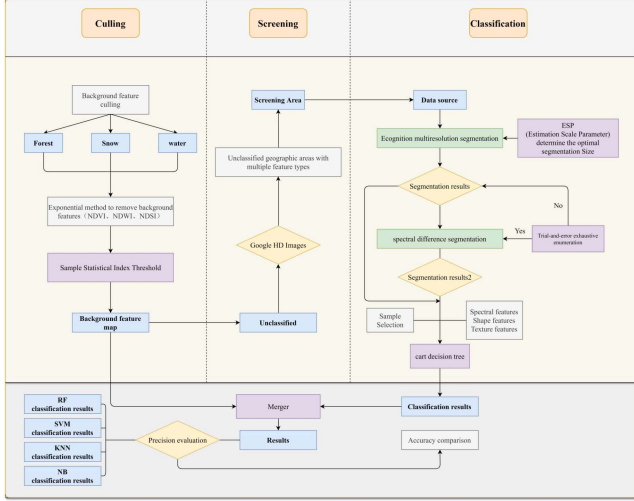


Fig. 2. Flow chart of the study.

water bodies, and snow cover in Zamu town throughout the year. It is worth noting that due to the substantial cloud coverage in Sentinel images over Zamu town, there are no images with an annual cloud volume of 20% or less. Hence, maximizing synthesis becomes crucial to retain as much feature information as possible.

To analyze the threshold range of each index, we collected sample points for the three land classes using Google HD imagery.

C Object-Oriented Cart Decision Tree Classification Process

1) *Image segmentation principle*: Multiscale segmentation is used to segment the image at different scales, allowing for a more comprehensive and accurate feature information extraction. This segmentation method can overcome the segmentation errors caused by different sizes and shapes of features in single-scale segmentation. It involves merging adjacent pixels or small segmented objects to ensure minimal average heterogeneity between entities while maximizing the homogeneity within each object [44], [45]. Heterogeneity is calculated as follows:

$$f = W_{\text{color}}h_{\text{color}} + W_{\text{shape}}h_{\text{shape}} \quad (1)$$

$$h_{\text{shape}} = W_{\text{compact}}h_{\text{compact}} + W_{\text{smooth}}h_{\text{smooth}} \quad (2)$$

Where f is the heterogeneity; W_{color} is the spectral information weight; W_{shape} is the shape information weight; the sum of these two weights is 1; h_{color} is the value of spectral heterogeneity; h_{shape} is the value of shape heterogeneity; W_{compact} and W_{smooth} are the weights of tightness and smoothness, respectively, and their sum is 1; h_{compact} and h_{smooth} are the heterogeneity values of tightness and smoothness, respectively [46].

2) *Spectral difference segmentation*: To classify different land cover features in remote sensing imagery, this method starts by extracting the spectral characteristics of various objects. First, it obtains reflectance values from other bands using multispectral images. Then, it calculates the reflectance differences for each

pixel across the different bands, resulting in a spectral feature space. Clustering is applied based on the distances between image elements in the spectral feature space. This process groups similar elements. Ultimately, the remote sensing images are segmented into distinct feature classes. This study employs the method as an optimization tool for segmentation. Based on a multiscale segmentation algorithm that analyzes the differences in spectral features of neighboring segmented objects to decide whether to merge the neighboring objects [47]. The spectral difference (g) is calculated as follows:

$$g = W_{b_1} \cdot |b_{1_1} - b_{1_2}| + W_{b_2} \cdot |b_{2_1} - b_{2_2}| + W_{b_3} \cdot |b_{3_1} - b_{3_2}| \quad (3)$$

Where b_{1_1} , b_{1_2} , and b_{1_3} denote the three bands of the image, respectively. W_{b_1} , W_{b_2} , and W_{b_3} are the normalized weights of the three bands, respectively. The normalization is calculated as follows:

$$W_{b_1} = W_{b_1} / (W_{b_1} + W_{b_2} + W_{b_3}) \quad (4)$$

$$W_{b_2} = W_{b_2} / (W_{b_1} + W_{b_2} + W_{b_3}) \quad (5)$$

$$W_{b_3} = W_{b_3} / (W_{b_1} + W_{b_2} + W_{b_3}). \quad (6)$$

The spectral difference segmentation method leverages the spectral information in remote sensing images more efficiently, making it particularly effective in classifying features with distinct spectral differences [48]. However, when there are only minor spectral differences between features in the image, it can potentially affect classification accuracy [49].

3) *Cart decision trees*: Cart decision tree classification is a nonparametric statistical learning method employing a tree structure for classification and regression tasks. The fundamental principle of Cart decision tree classification involves iteratively selecting the most optimal features, partitioning the data, constructing a binary decision tree, and ultimately deriving a decision tree that enables classification determination. [50].

In Cart decision trees, the Gini index or information gain is typically used as the criterion for classifying attributes. The Gini index measures the impurity of the sample set and is commonly used in classification problems. If all the samples belong to the same category for the sample set D , then the Gini index is 0. If the samples are uniformly distributed in each category, then the Gini index reaches the maximum value 1. The formula is

$$G = \sum_{i=1}^c p(i) \cdot [1 - p(i)] \quad (7)$$

where G is the Gini coefficient, $p(i)$ is the probability of a sample being classified into category i , and C is the number of categories.

Information gain is a metric that quantifies a sample set's impurity reduction and is commonly employed in classification and regression problems. In the context of a sample set D , its information entropy can be defined as

$$H(D) = - \sum_{k=1}^k \frac{|C_k|}{|D|} \log_2 \frac{|C_k|}{|D|}. \quad (8)$$

$H(D)$ is the information entropy, C_k denotes the number of categories belonging to the k th category, and the sum of the numbers of all categories of C .

In the Cart algorithm, training sample selection typically employs two prevalent methods.

- 1) *Random selection*: This method involves drawing a specific number of samples randomly from the dataset to construct the classification tree. Such randomness ensures the training set's representativeness and reduces potential biases. Although this method conserves computational effort, it might introduce some volatility into the classification tree.
- 2) *Selection by sample weights*: Samples are chosen based on their weights to construct the classification tree, enhancing its stability. While this approach demands the computation of weights for each sample, increasing the computational load, it proves advantageous when dealing with imbalanced datasets or when certain samples have heightened importance.

In our study, after sidelining numerous background features, the emphasis shifted to classifying specific areas. Samples were selected based on weights attributed to diverse land types, derived from segmentation outcomes. Classification focused on eight distinct classes: forest, road, unused, farm, building, gravel, water, and snow. Google HD images, in tandem with the eCognition Developer 9.0 platform, guided the sample selection under this classification schema, ensuring a balanced representation of each land type and fostering precise classification outcomes.

Feature metric selection is pivotal in decision tree classification, with its quality directly influencing classification accuracy. Spectrum, shape, and texture are among the routinely employed feature metrics [46], [51]. Given the novelty of object-oriented extraction methods in gravel research, our study harnessed the Greedy Algorithm for feature metric selection. This optimization strategy, rooted in a greedy paradigm, continually opts for the best current choice, aspiring for an optimal global solution [52]. In the realm of feature selection, the Greedy Algorithm persistently selects the prime feature combination, expediting the search and optimization of the feature space.

Drawing from this and integrating with pertinent Cart decision tree classification research, we selected 24 features spanning spectral, shape, texture, and custom domains. Spectral features encompass seven mean band values synthesized from Google HD and Sentinel images. Shape features spotlight metrics such as length/width, compactness, shape index, and rectangular fit. Texture features pivot around the gray-level co-occurrence matrix (GLCM), a widely recognized texture descriptor capturing the spatial interplay between varying gray levels in an image [42]. GLCM indices, including mean, entropy, homogeneity, dissimilarity std dev, contrast, and correlation, are harnessed for texture features. Custom features, meanwhile, utilize indices such as NDVI, NDWI, NDSI, normalized difference built-up index), MNDWI (Modified NDWI), and BSI (bare soil index).

IV. RESULT

A. Background Feature Rejection

The annual NDVI, NDSI, and NDWI were obtained using the maximum synthesis method. For each feature type (forest, snow, and water), 417, 354, and 332 sample points were selected

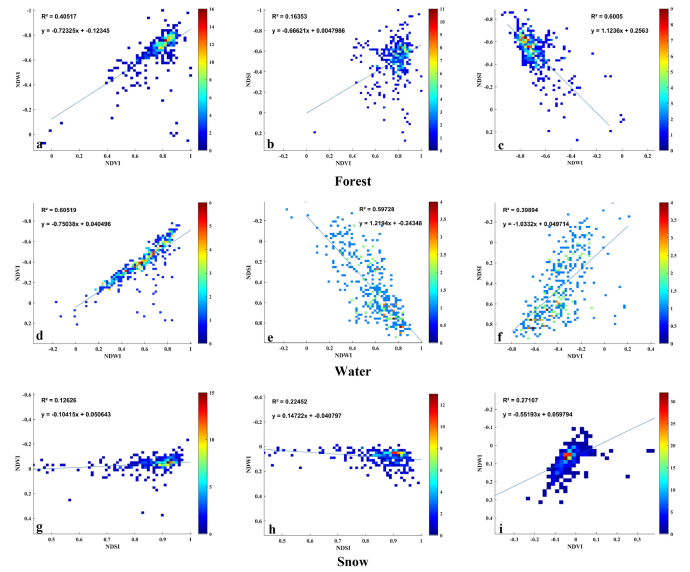


Fig. 3. NDVI, NDWI, NDSI index distribution of forest, snow, and water land types.

TABLE I
NDVI, NDWI, AND NDSI INDEX THRESHOLDS FOR FOREST, WATER, AND SNOW TYPES

	NDVI	NDWI	NDSI
Forest	0.39–Max	-0.4 to Min	-0.38 to Min
Water	-0.2 to 0.39	0.2–max	0.15–0.6
Snow	-0.1–0.1	0–0.2	0.6–max

based on Google HD historical images from January 13, 2020. According to Fig. 3(a), (b), and (c), the clustering intervals of NDVI, NDWI, and NDSI for forest are 0.39–Max, -0.4 –Min, and -0.38 –Min, respectively; similarly, according to Fig. 3(d), (e), and (f) and Fig. 3(g), (h), and (i), the clustering intervals of NDVI, NDWI and NDSI for water and snow are respectively, The values of NDVI, NDWI, and NDSI for snow are -0.2 to 0.39 , 0.2 –max, 0.15 – 0.6 ; -0.1 to 0.1 , 0 – 0.2 , 0.6 –max, respectively (refer to Table I for details). The extraction indices for each site are determined according to the correlation between indices and specific situations. Extraction forest was dominated by indices NDVI and NDWI, water was dominated by NDVI and NDWI, and snow was dominated by NDSI and NDWI.

Fig. 4(a), (b), and (c) illustrates the extraction effect of a single index (e.g., NDVI) specifically for the forest class. However, when extracting the three land class categories (forest, water, and snow), misclassifications of other land classes may occur. To address this issue, additional indices are incorporated to improve the accuracy of the classification. The resulting figures, Fig. 4(d), (e), and (f), demonstrate the extraction effect after combining multiple indices. The background feature map can be obtained by combining the corrected three features in Fig. 5. A total of 12 sample areas are selected for object-oriented Cart decision tree extraction of features according to Fig. 5.

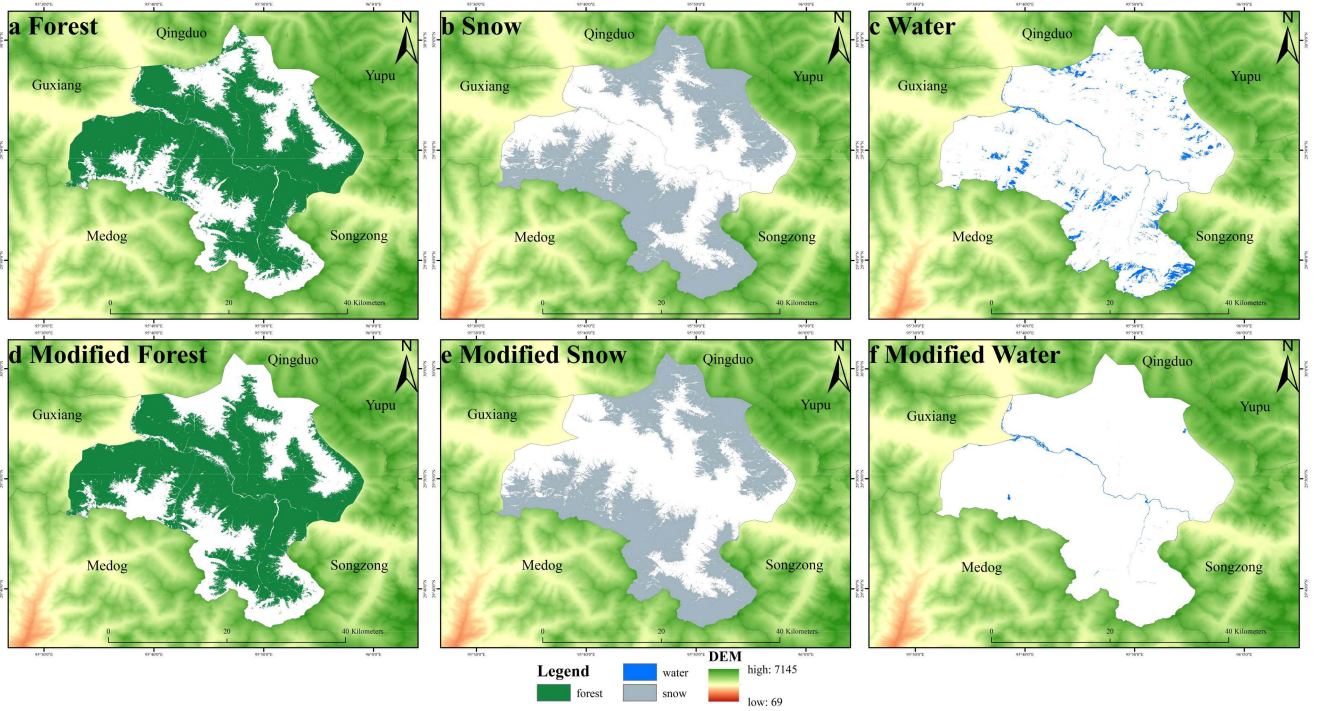


Fig. 4. Extraction and modification of background features such as forest, snow, and water.

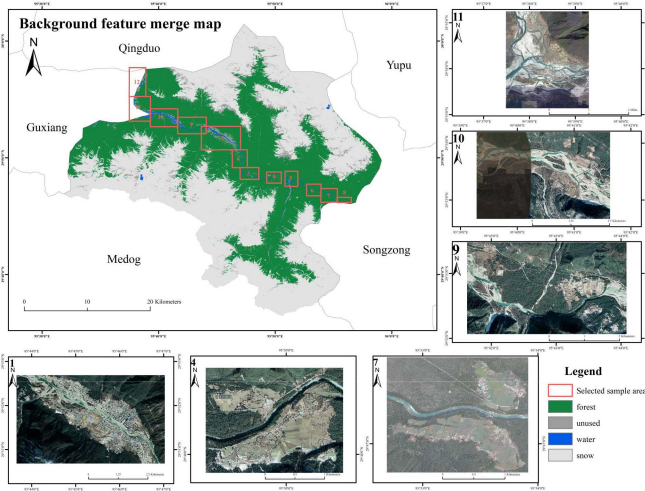


Fig. 5. Synthesis of background features and selection of the sample area to be selected.

TABLE II

EACH PARAMETER OF MULTIREOLUTION SEGMENTATION AND SPECTRAL DIFFERENCE SEGMENTATION

ID	multiresolution segmentation			spectral difference segmentation
	Scale parameter	Shape	Compactness	Maximum spectral different
1	75	0.3	0.5	5
2	75	0.3	0.5	5
3	80	0.1	0.5	2
4	74	0.2	0.5	2
5	32	0.1	0.5	5
6	63	0.2	0.5	5
7	84	0.1	0.5	1
8	45	0.1	0.5	1
9	40	0.2	0.5	1
10	55	0.1	0.5	5
11	75	0.3	0.5	
12	58	0.2	0.5	2

B. Determination of the Optimal Segmentation Scale

In object-oriented feature extraction, selecting the optimal segmentation scale is a crucial parameter that determines the size and shape of the segmented objects [51], [53], [54]. We determined the optimal segmentation scale through trial and error using the ESP2 (Estimation_Scale_Parameter) plugin based on eCognition Developer 9.0, resulting in the findings presented in Table II. In the multiresolution segmentation, the weight proportions of each band were set as 0.5, 1, 1, 1, 0.5, 0.5, 0.5. This adjustment was made because the r, g, b bands of Google

high-resolution images possess higher clarity and superior quality, thus their weights were appropriately increased. In the spectral difference segmentation, the weight proportions for each band were 1, 1, 1, 1, 1, 1, 1. This uniform distribution was employed because spectral difference segmentation determines whether merging should occur based on the spectral feature differences of adjacent units [55], [56], [57], it is crucial to keep the weights of each band consistent.

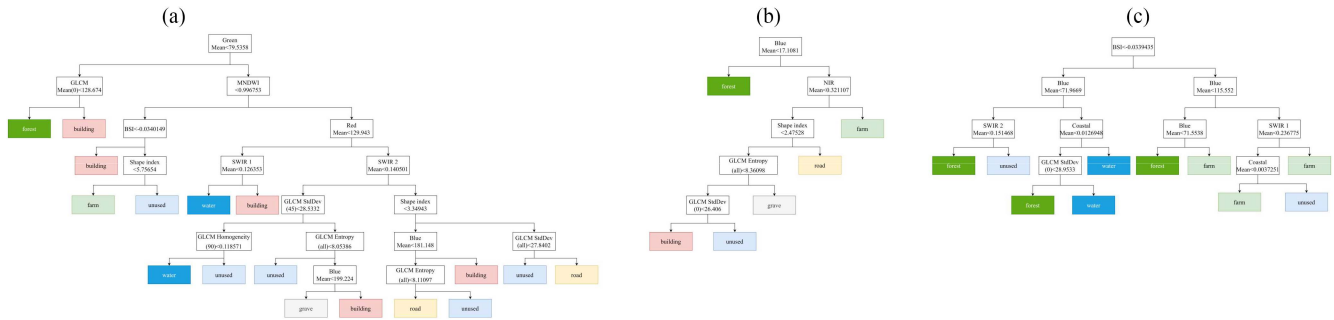


Fig. 6. Decision tree construction for the sample area. Sample regions 1, 2, 3, 4, and 5 correspond to the classification rules in (a). Sample regions 6, 7, and 8 correspond to (b), and sample regions 9, 10, 11, and 12 correspond to (c).

C. Image Classification and Decision Tree Construction

eCognition provides a highly automated decision tree classifier that utilizes the 24 selected feature indices to generate classification rules through Cart decision tree classification. However, different sample selection approaches are required due to variations in image quality, landscape features, feature characteristics, and segmentation scales among the selected sample areas. Therefore, the sample areas are divided into three categories, and different classification rules are generated based on the differences between the images. These classification rules are depicted in Fig. 6, where sample areas 1, 2, 3, 4, and 5 correspond to Fig. 6(a), sample areas 6, 7, and 8 correspond to Fig. 6(b), and sample areas 9, 10, 11, and 12 correspond to Fig. 6(c).

Analyzing Fig. 6 reveals that spectral features play a dominant role (47.6%) in the classification of land classes, followed by texture features (38.1%). The only custom features that contribute to the construction of classification rules are BSI and MNDWI. The introduction of additional features is limited because they have weak connections to this study, and the spectral band of Sentinel 2 exhibits calculation errors that affect its response to the feature conditions.

Among the sample areas, 1, 2, 3, 4, and 5 exhibit confusion between building and unused land classes, while forest and gravel classes are better distinguished. The presence of diverse types of houses in the area and the varied characteristics of adjacent unused land (such as bare land around rivers, open land around buildings, and bare land on hillsides) make it challenging to differentiate between these two land classes. In contrast, the rules for classifying forest are simpler due to its uniform type and concentrated distribution.

Sample areas 6, 7, and 8 exhibit more distinct clustering characteristics and simpler feature types. However, the presence of large shadows in the area negatively impacts the classification of land classes. Visual interpretation can be employed later to improve the accuracy of the classification. Sample areas 9, 10, 11, and 12 primarily consist of woodland with large-scale distribution. The extraction rules for these areas are relatively simpler and less challenging compared to the decision trees in sample areas 1, 2, 3, 4, and 5.

Based on the trained classification rules depicted in Fig. 6, a map illustrating the classification of each sample area can be obtained [see Fig. 7(a)].

D. Accuracy Evaluation and Result Analysis

To gauge the accuracy of the object-oriented Cart decision tree classification outcomes, a supervised classification was executed using Sentinel 2 images on the GEE platform, with a primary focus on classifiers by using KNN, RF, SVM, and NB. This supervised classification on GEE incorporated 7 bands of Sentinel 2 data and 6 custom feature indices from the Cart decision tree. The outcomes of this classification are depicted in Fig. 7.

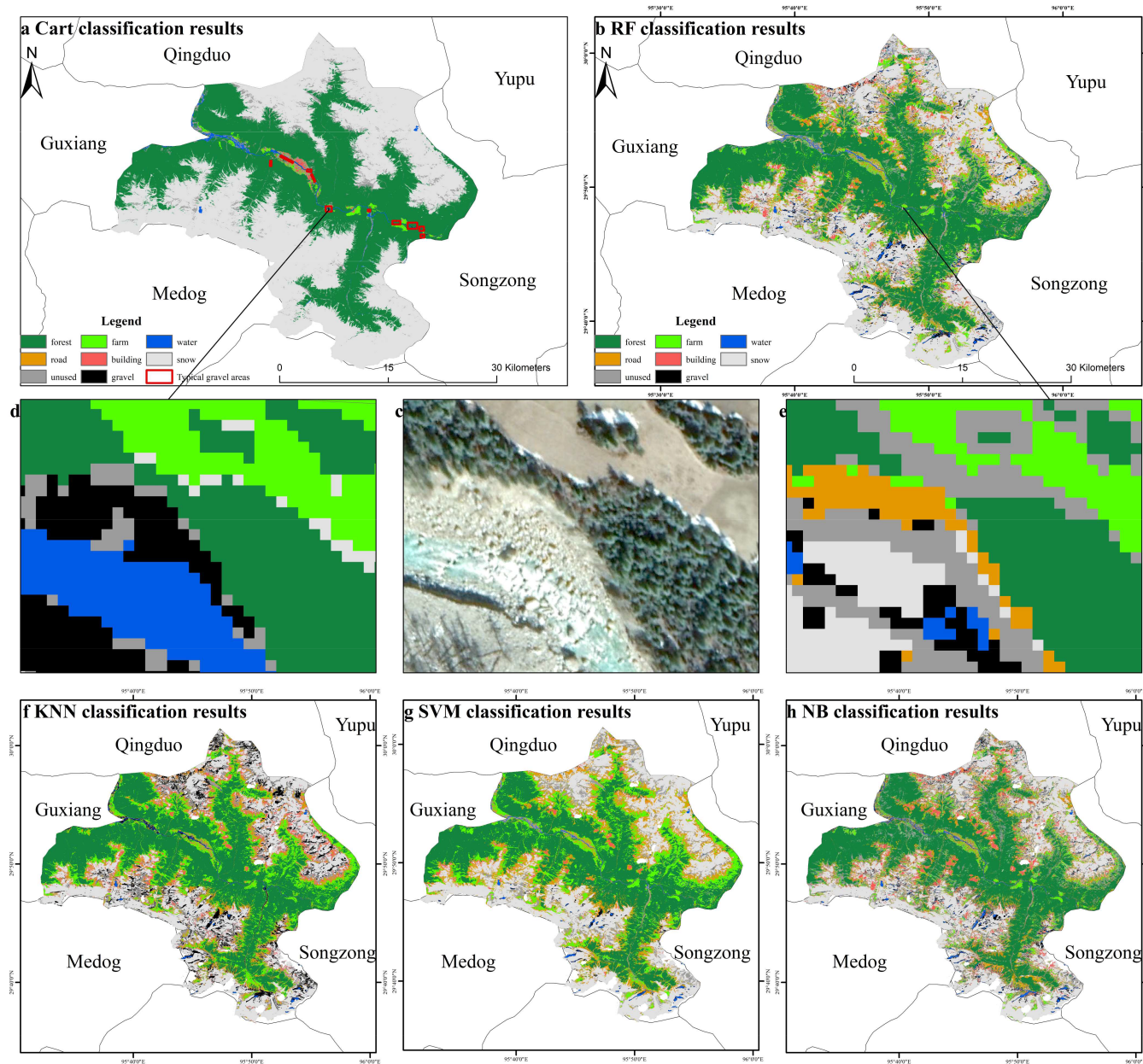
Upon examining Fig. 7, one discerns that the classification outcomes, postfiltering and merging, manifest as more structured and aggregated. Conversely, the supervised classification outcomes display a higher incidence of misclassifications. Notably, in the extraction of the target feature (gravel), the object-oriented Cart decision tree method demonstrates superior accuracy compared to the supervised classification on GEE, as detailed in Table III.

Table III presents the confusion matrices for both classification outcomes. Evaluating the accuracy data in Table III reveals that both the user accuracy and producer accuracy for the land class divisions, as determined by the Cart decision tree algorithm, predominantly exceed 0.8. An exception is the “Unused” category, which registers an accuracy below 0.7. In juxtaposition, other supervised classification methods exhibit diminished overall accuracy and Kappa coefficients, with only the RF classifier surpassing an overall accuracy of 0.6. This underscores the need for enhancing the accuracy of supervised classification outcomes based on GEE.

The Cart decision tree’s overall accuracy and Kappa coefficient surpass 0.8. In the realm of supervised classification, merely the RF classifier’s overall accuracy hovers between 0.6 and 0.7. When focusing on the extraction of the target feature (continuous gravel areas), the Cart decision tree algorithm outperforms the RF algorithm in terms of accuracy and precision. This underscores the efficacy and precision of the Cart decision tree classification method, anchored in the “reject, filter, classify, and merge” paradigm, for gravel extraction.

V. DISCUSSION

Removing the feature background reduces noise and interference, thereby improving the accuracy and reliability of target detection and identification. The use of Google HD historical



c shows a typical gravel contiguous area, and d and e show the extraction effect of different extraction methods (decision tree, random forest)

Fig. 7. Comparison of decision tree classification results with those obtained from other supervised classifiers. (a) represents the object-oriented classification results based on the Cart decision tree. (b), (f), (g), and (h) represent the classification results obtained from different supervised classifiers, namely Random Forest (RF), k-Nearest Neighbors (KNN), Support Vector Machine (SVM), and Naive Bayes (NB) respectively. (c) shows high-resolution Google imagery of a typical gravel distribution area. (d) and (e) correspond to the classification results of Cart and RF, respectively (in the same area as (c)).

images for index sample selection ensures the accuracy of each feature within the specified time range and serves as a basis for determining index thresholds. However, removing feature backgrounds requires considering various factors such as image resolution, feature type, lighting conditions, weather, etc. These factors collectively impact the removal effectiveness and need to be carefully considered and optimized [56], [58], [59]. In this study, it was observed that the selection of feature samples in shaded areas and the classification of features had a negative effect on the accuracy of feature classification. In addition, the low quality and high cloudiness of the Sentinel data resulted in

the calculation of background feature thresholds based on the maximum index value, which conflicted with the time range of the Google HD images (January 13, 2020) and posed a challenge to the accuracy of subsequent results (due to the cloud cover exceeding 30% in the Sentinel-2 data throughout the year 2020 in GEE and the poor data quality, selecting only the Sentinel images that align with the Google HD historical images from January 13, 2020, would significantly compromise the data availability. Therefore, to err on the side of caution, we chose to merge the Sentinel images synthesized throughout the year with the Google HD historical images.). Moreover, the

TABLE III
CLASSIFICATION ACCURACY EVALUATION OF DIFFERENT CLASSIFIERS

Category		forest	road	unused	farm	building	grave	water	snow
classification and regression tree	Producer's Accuracy	80.00%	90.00%	68.00%	93.94%	88.89%	100.00%	80.95%	89.58%
	User's Accuracy	90.91%	75.00%	60.71%	88.57%	84.21%	77.78%	100.00%	89.58%
	Overall accuracy	84.91%							
	kappa	82.01%							
Random Forest Algorithm	Producer's Accuracy	86.84%	35.71%	48.39%	60.42%	61.54%	44.44%	81.25%	88.89%
	User's Accuracy	75.00%	45.45%	57.69%	93.55%	42.11%	44.44%	76.47%	66.67%
	Overall accuracy	67.80%							
	kappa	61.10%							
Naive Bayes	Producer's Accuracy	85.71%	33.33%	26.47%	80.56%	52.63%	66.67%	80.00%	81.58%
	User's Accuracy	72.00%	45.45%	45.00%	93.55%	52.63%	44.44%	70.59%	64.58%
	Overall accuracy	66.34%							
	kappa	59.33%							
Support Vector Machines	Producer's Accuracy	86.11%	17.24%	62.50%	43.48%	42.86%	60.00%	100.00%	93.55%
	User's Accuracy	62.00%	45.45%	50.00%	66.77%	15.70%	33.33%	70.59%	60.42%
	Overall accuracy	60.00%							
	kappa	51.67%							
K-Nearest Neighbors algorithm	Producer's Accuracy	76.74%	41.67%	31.25%	41.82%	58.33%	10.00%	81.25%	93.33%
	User's Accuracy	66.00%	45.45%	25.00%	74.19%	38.89%	22.22%	76.47%	58.33%
	Overall accuracy	56.86%							
	kappa	47.78%							

classification of background features in this study was relatively coarse, enhancing calculation efficiency but failing to consider subcategory subdivisions. In the extraction of background features, relying solely on a single index may yield unsatisfactory results, necessitating the combination of multiple indices to improve the accuracy and reliability of feature extraction.

The ESP can determine the scale of multiresolution segmentation, but parameters such as shape and compactness can only be determined through trial. Similarly, the parameters for spectral difference segmentation are determined empirically. However, the selected segmentation scale for spectral difference segmentation tends to be small due to the influence of feature type and sample area. This is because some sample areas have a limited number of feature types, and different features are closely clustered together. Increasing the segmentation scale in such cases would lead to the mixing of other features within the segmentation units [46], [60].

The greedy algorithm is employed for decision tree construction. Although adding more extracted features does not significantly impact the construction of the optimal decision tree, reducing unnecessary feature input can enhance extraction efficiency and automation. The exponential features introduced in this study play a minor role in formulating classification rules. The extraction of target features (gravel) primarily relies on visible band and texture features. Therefore, improving the inclusion of features in a reasonable manner becomes a way to enhance classification efficiency. In addition, the limitations imposed by data accuracy result in the ineffective integration of index features into the formulation of classification rules, as

they are unable to accurately depict true features. On the other hand, visible band and texture features heavily rely on Google HD images, rendering them more dependable and capable of accurately representing land features. This, in turn, enhances their influence in the creation of decision tree classification rules.

Similarly, the Cart decision tree classification method based on the concept of “cull, filter, classify, and merge” also faces considerable constraints in its applicability. On one hand, the removal of background features requires them to be a single continuous cover of a specific land type. Hence, the applicable area is limited to regions with large coverage of single-type background features and relatively simple land types for target extraction within small scopes. Under these conditions, the method is less suitable for areas with complex land type distributions.

The culminating classification outcomes underscore the efficacy of the Cart decision tree classification method, rooted in the “cull, filter, classify, and merge” philosophy, over the conventional supervised classification method epitomized by the RF Algorithm. This edge is largely due to the prevalence of snow and woodland in the study area. By sidelining pure pixels in these terrains, the sample selection process remains largely unencumbered by external interferences, simplifying classification. Moreover, this feature exclusion paves the way for geographic classification, facilitating the generation of a comprehensive geographic classification map for the entire study area during subsequent merging. Focusing on discrete small-area scopes curtails land classification’s computational complexity, while the merits of object-oriented land classification for high-resolution, small-scale geographic areas come to the fore [59], [60]. When

extending the classification scope to encompass the entirety of Bomi County using this methodology, it became evident that background feature removal was effective. However, the data source for supervised classification is anchored in the Sentinel-2 dataset. Given the region's pronounced cloud cover and diminished image resolution, sample selection often encompasses mixed pixels, especially when pinpointing samples for built-up areas. This invariably results in pronounced misclassification and omission errors.

VI. CONCLUSION

In this article, an object-oriented approach was used to construct the Cart decision tree model for gravel extraction in Zamu town. The following conclusions were drawn.

- 1) Culling background features have significant advantages in image feature classification. The exponential thresholding method was used to identify features with a large area distribution, which effectively reduced the computational effort of the object-oriented approach. Thresholds for NDVI, NDWI, and NDSI were determined for forest, snow, and water features in Zamu town. The thresholds for NDVI, NDWI, and NDSI for the forest class are 0.39–Max, -0.4 to Min, and -0.38 to Min respectively. For the snow class, the thresholds for NDVI, NDWI, and NDSI are -0.1 to 0.1, 0–0.2, and 0.6–Max, respectively. For the water class, the thresholds for NDVI, NDWI, and NDSI are -0.2 to 0.39, 0.2–Max, and 0.15–0.6, respectively. The extraction through the index method serves both as a filter for background features and as a means of classification. It effectively defines the range for pure pixels. However, its application is less effective in areas with complex and diverse land cover distributions and abundant attributes.
- 2) Compared to the traditional RF algorithm, the Cart extraction method used in this study showed higher accuracy after background feature screening. The producer accuracy of the target feature was 2.27 times higher than that of the RF algorithm, and the user accuracy was 1.75 times higher. The overall accuracy was 1.25 times higher, and the Kappa value was 1.34 times higher. These results demonstrate that the Cart extraction method is accurate and reliable for gravel extraction.
- 3) In small-scale gravel extraction, spectral features played a dominant role in terrain classification (47.6%), followed by textural features (38.1%). Texture features and spectral features exhibited better discriminatory abilities, while the introduction of various indices did not contribute significantly. Among them, the Blue band and features screened by GLCM entropy showed good distinguishing effects for gravel extraction. These findings provide a basis for future studies on extracting small-scale features in large study areas.

ACKNOWLEDGMENT

The authors would like to thank the researchers who provide the datasets. Also, we acknowledge the handling editor and the anonymous reviewers for their critical and constructive comments in dealing with this manuscript.

REFERENCES

- [1] H. Matsumoto and A. P. Young, "Quantitative regional observations of gravel and bedrock influence on beach morphologies," *Geomorphology*, vol. 419, 2022, Art. no. 108491.
- [2] S. Beck-Broichsitter, Z. H. Rizvi, R. Horn, and F. Wuttke, "Effect of gravel content on soil water retention characteristics and thermal capacity of sandy and silty soils," *J. Hydrol. Hydromechanics*, vol. 71, no. 1, pp. 1–10, 2023.
- [3] L. Liu, J. Zhou, D. Jiang, D. Zhuang, and L. R. Mansaray, "Lithological discrimination of the mafic-ultramafic complex, huitongshan, beishan, China: Using ASTER data," *J. Earth Sci.*, vol. 25, pp. 529–536, 2014.
- [4] C. Dai, W. Li, D. Wang, H. Lu, Q. Xu, and J. Jian, "Active landslide detection based on sentinel-1 data and InSAR technology in Zhouqu county, Gansu province, northwest China," *J. Earth Sci.*, vol. 32, pp. 1092–1103, 2021.
- [5] L. Meyer, C. Johnson, and G. Foster, "Stone and woodchip mulches for erosion control on construction sites," *J Soil Water Conservation*, vol. 27, pp. 264–269, 1972.
- [6] L. Pavlů, R. Kodešová, M. Fér, A. Nikodem, F. Němec, and R. Prokeš, "The impact of various mulch types on soil properties controlling water regime of the haplic fluvisol," *Soil Tillage Res.*, vol. 205, 2021, Art. no. 104748.
- [7] M. Bendixen et al., "Sand, gravel, and UN sustainable development goals: Conflicts, synergies, and pathways forward," *One Earth*, vol. 4, no. 8, pp. 1095–1111, 2021.
- [8] C. D. Wilson, D. Roberts, and N. Reid, "Applying species distribution modelling to identify areas of high conservation value for endangered species: A case study using *Margaritifera margaritifera* (L.)," *Biol. Conservation*, vol. 144, no. 2, pp. 821–829, 2011.
- [9] G. Zauner, M. Jung, C. Ratschan, and M. Mühlbauer, "Ecological restoration of free flowing and impounded stretches of the Austrian Danube river—towards the objectives of the water framework directive," *Österreichische Wasser Abfallwirtschaft*, vol. 68, pp. 503–518, 2016.
- [10] G. M. Kondolf, "Geomorphic and environmental effects of instream gravel mining," *Landscape Urban Plan.*, vol. 28, no. 2–3, pp. 225–243, 1994.
- [11] S. Nadeau, E. Rosa, V. Cloutier, R.-A. Daigneault, and J. Veillette, "A GIS-based approach for supporting groundwater protection in eskers: Application to sand and gravel extraction activities in Abitibi-Témiscamingue, Quebec, Canada," *J. Hydrol., Regional Stud.*, vol. 4, pp. 535–549, 2015.
- [12] M. V. Podimata and P. C. Yannopoulos, "A conceptual approach to model sand–gravel extraction from rivers based on a game theory perspective," *J. Environ. Plan. Manage.*, vol. 59, no. 1, pp. 120–141, 2016.
- [13] J. Zawiejska, B. Wyżga, and A. Radecki-Pawlik, "Variation in surface bed material along a mountain river modified by gravel extraction and channelization, the Czarny Dunajec, Polish Carpathians," *Geomorphology*, vol. 231, pp. 353–366, 2015.
- [14] J. Liu, Q. Qin, J. Li, and Y. Li, "Rural road extraction from high-resolution remote sensing images based on geometric feature inference," *ISPRS Int. J. Geo-Inf.*, vol. 6, no. 10, 2017, Art. no. 314.
- [15] M. Lorang, D. Whited, F. Hauer, J. Kimball, and J. A. Stanford, "Using airborne multispectral imagery to evaluate geomorphic work across floodplains of gravel-bed rivers," *Ecological Appl.*, vol. 15, no. 4, pp. 1209–1222, 2005.
- [16] D. C. Diaconu, P. D. Koutalakis, G. T. Gkiatas, G. V. Dascalu, and G. N. Zaimes, "River sand and gravel mining monitoring using remote sensing and UAVs," *Sustainability*, vol. 15, no. 3, 2023, Art. no. 1944.
- [17] C. Shintani and M. A. Fonstad, "Comparing remote-sensing techniques collecting bathymetric data from a gravel-bed river," *Int. J. Remote Sens.*, vol. 38, no. 8–10, pp. 2883–2902, 2017.
- [18] N. Gorelick, M. Hancher, M. Dixon, S. Ilyushchenko, D. Thau, and R. Moore, "Google Earth Engine: Planetary-scale geospatial analysis for everyone," *Remote Sens. Environ.*, vol. 202, pp. 18–27, 2017.
- [19] M. A. P. Aji, M. Kamal, and N. M. Farda, "Mangrove species mapping through phenological analysis using random forest algorithm on Google Earth Engine," *Remote Sens. Appl.: Soc. Environ.*, vol. 30, 2023, Art. no. 100978.
- [20] D. Parastatidis, Z. Mitraka, N. Chrysoulakis, and M. Abrams, "Online global land surface temperature estimation from landsat," *Remote Sens.*, vol. 9, no. 12, 2017, Art. no. 1208.
- [21] F. Masoumi, T. Eslamkish, A. A. Abkar, M. Honarmand, and J. R. Harris, "Integration of spectral, thermal, and textural features of ASTER data using random forests classification for lithological mapping," *J. Afr. Earth Sci.*, vol. 129, pp. 445–457, 2017.

- [22] F. Li, X. Li, W. Chen, Y. Dong, Y. Li, and L. Wang, "Automatic lithology classification based on deep features using dualpolarization SAR Images," *Earth Sci.*, vol. 47, no. 11, pp. 4267–4279, 2022.
- [23] S. Grebby, E. Field, and K. Tansey, "Evaluating the use of an object-based approach to lithological mapping in vegetated terrain," *Remote Sens.*, vol. 8, no. 10, pp. 843, 2016.
- [24] S. Bar, B. R. Parida, and A. C. Pandey, "Landsat-8 and Sentinel-2 based Forest fire burn area mapping using machine learning algorithms on GEE cloud platform over Uttarakhand, western Himalaya," *Remote Sens. Appl., Soc. Environ.*, vol. 18, 2020, Art. no. 100324.
- [25] X. Sang et al., "Intensity and stationarity analysis of land use change based on CART algorithm," *Sci. Rep.*, vol. 9, no. 1, 2019, Art. no. 12279.
- [26] Y. Zhao, D. Chen, and F. Fan, "Sustainable development problems and countermeasures: A case study of the Qinghai-Tibet plateau," *Geogr. Sustainability*, vol. 1, no. 4, pp. 275–283, 2020.
- [27] F. U. B. et al., "Current condition and protection strategies of Qinghai-Tibet Plateau ecological security barrier," *Bull. Chin. Acad. Sci. (Chin. Version)*, vol. 36, no. 11, pp. 1298–1306, 2021.
- [28] R. Wei et al., "Geohazard cascade and mechanism of large debris flows in Tianmo gully, SE Tibetan Plateau and implications to hazard monitoring," *Eng. Geol.*, vol. 233, pp. 172–182, 2018.
- [29] J. Yang and X. Huang, "30 m annual land cover and its dynamics in China from 1990 to 2019," *Earth System Sci. Data Discuss.*, vol. 2021, pp. 1–29, 2021.
- [30] N. Pettorelli, J. O. Vik, A. Mysterud, J.-M. Gaillard, C. J. Tucker, and N. C. Stenseth, "Using the satellite-derived NDVI to assess ecological responses to environmental change," *Trends Ecol. Evol.*, vol. 20, no. 9, pp. 503–510, 2005.
- [31] D. K. Hall, G. A. Riggs, and V. V. Salomonson, "Development of methods for mapping global snow cover using moderate resolution imaging spectroradiometer data," *Remote Sens. Environ.*, vol. 54, no. 2, pp. 127–140, 1995.
- [32] H. Xu, "Modification of normalised difference water index (NDWI) to enhance open water features in remotely sensed imagery," *Int. J. Remote Sens.*, vol. 27, no. 14, pp. 3025–3033, 2006.
- [33] M. Pal and P. M. Mather, "Support vector machines for classification in remote sensing," *Int. J. Remote Sens.*, vol. 26, no. 5, pp. 1007–1011, 2005.
- [34] A. Romero, C. Gatta, and G. Camps-Valls, "Unsupervised deep feature extraction for remote sensing image classification," *IEEE Trans. Geosci. Remote Sens.*, vol. 54, no. 3, pp. 1349–1362, Mar. 2015.
- [35] J. M. Bioucas-Dias et al., "Hyperspectral unmixing overview: Geometrical, statistical, and sparse regression-based approaches," *IEEE J. Sel. Topics Appl. Earth Observ. Remote Sens.*, vol. 5, no. 2, pp. 354–379, Apr. 2012.
- [36] M. Belgiu and L. Drăguț, "Random forest in remote sensing: A review of applications and future directions," *ISPRS J. Photogramm. Remote Sens.*, vol. 114, pp. 24–31, 2016.
- [37] M. Pal and P. M. Mather, "An assessment of the effectiveness of decision tree methods for land cover classification," *Remote Sens. Environ.*, vol. 86, no. 4, pp. 554–565, 2003.
- [38] D. I. Enderle and R. C. Weih, "Integrating supervised and unsupervised classification methods to develop a more accurate land cover classification," *J. Arkansas Acad. Sci.*, vol. 59, no. 1, pp. 65–73, 2005.
- [39] S. Bhattacharya, T. R. Carr, and M. Pal, "Comparison of supervised and unsupervised approaches for mudstone lithofacies classification: Case studies from the Bakken and Mahantango-Marcellus Shale, USA," *J. Natural Gas Sci. Eng.*, vol. 33, pp. 1119–1133, 2016.
- [40] T. Blaschke et al., "Geographic object-based image analysis—towards a new paradigm," *ISPRS J. Photogramm. Remote Sens.*, vol. 87, pp. 180–191, 2014.
- [41] R. Mathieu, J. Aryal, and A. K. Chong, "Object-based classification of Ikonos imagery for mapping large-scale vegetation communities in urban areas," *Sensors*, vol. 7, no. 11, pp. 2860–2880, 2007.
- [42] D. Chen, D. Stow, and P. Gong, "Examining the effect of spatial resolution and texture window size on classification accuracy: An urban environment case," *Int. J. Remote Sens.*, vol. 25, no. 11, pp. 2177–2192, 2004.
- [43] D. Lu and Q. Weng, "A survey of image classification methods and techniques for improving classification performance," *Int. J. Remote Sens.*, vol. 28, no. 5, pp. 823–870, 2007.
- [44] G. J. Hay, G. Castilla, M. A. Wulder, and J. R. Ruiz, "An automated object-based approach for the multiscale image segmentation of forest scenes," *Int. J. Appl. Earth Observation Geoinf.*, vol. 7, no. 4, pp. 339–359, 2005.
- [45] P. Soille, *Morphological Image Analysis: Principles and Applications*. New York, NY, USA: Springer, 1999.
- [46] L. Zhang, K. Jia, X. Li, Q. Yuan, and X. Zhao, "Multi-scale segmentation approach for object-based land-cover classification using high-resolution imagery," *Remote Sens. Lett.*, vol. 5, no. 1, pp. 73–82, 2014.
- [47] Y. Tarabalka, J. Chanussot, J. A. Benediktsson, J. Angulo, and M. Fauvel, "Segmentation and classification of hyperspectral data using watershed," in *Proc. IEEE Int. Geosci. Remote Sens. Symp.*, 2008, pp. III–652–III–655.
- [48] R. Zhang and D. Zhu, "Study of land cover classification based on knowledge rules using high-resolution remote sensing images," *Expert Syst. Appl.*, vol. 38, no. 4, pp. 3647–3652, 2011.
- [49] M. De Martino, F. Causa, and S. B. Serpico, "Classification of optical high resolution images in urban environment using spectral and textural information," in *Proc. IEEE Int. Geosci. Remote Sens. Symp. Proc.*, 2003, pp. 467–469.
- [50] W. Y. Loh, "Classification and regression trees," *Wiley Interdiscipl. Rev., Data Mining Knowl. Discov.*, vol. 1, no. 1, pp. 14–23, 2011.
- [51] T. Kavzoglu, I. Colkesen, and T. Yomralioglu, "Object-based classification with rotation forest ensemble learning algorithm using very-high-resolution WorldView-2 image," *Remote Sens. Lett.*, vol. 6, no. 11, pp. 834–843, 2015.
- [52] A. Vince, "A framework for the greedy algorithm," *Discrete Appl. Math.*, vol. 121, no. 1–3, pp. 247–260, 2002.
- [53] R. Gaetano, G. Scarpa, and G. Poggi, "Hierarchical texture-based segmentation of multiresolution remote-sensing images," *IEEE Trans. Geosci. Remote Sens.*, vol. 47, no. 7, pp. 2129–2141, Jul. 2009.
- [54] K. Wu, G. Xu, Y. Zhang, and B. Du, "Hyperspectral image target detection via integrated background suppression with adaptive weight selection," *Neurocomputing*, vol. 315, pp. 59–67, 2018.
- [55] Y. Wu, X. Peng, K. Ruan, and Z. Hu, "Improved image segmentation method based on morphological reconstruction," *Multimedia Tools Appl.*, vol. 76, pp. 19781–19793, 2017.
- [56] G. M. Gandhi, B. Parthiban, N. Thummalu, and A. Christy, "Ndvi: Vegetation change detection using remote sensing and gis—A case study of Vellore district," *Procedia Comput. Sci.*, vol. 57, pp. 1199–1210, 2015.
- [57] X. X. Zhu et al., "Deep learning in remote sensing: A comprehensive review and list of resources," *IEEE Geosci. Remote Sens. Mag.*, vol. 5, no. 4, pp. 8–36, Dec. 2017.
- [58] A. Sharma, X. Liu, and X. Yang, "Land cover classification from multi-temporal, multi-spectral remotely sensed imagery using patch-based recurrent neural networks," *Neural Netw.*, vol. 105, pp. 346–355, 2018.
- [59] T. Blaschke, "Object based image analysis for remote sensing," *ISPRS J. Photogramm. Remote Sens.*, vol. 65, no. 1, pp. 2–16, 2010.
- [60] U. C. Benz, P. Hofmann, G. Willhauck, I. Lingenfelder, and M. Heynen, "Multi-resolution, object-oriented fuzzy analysis of remote sensing data for GIS-ready information," *ISPRS J. Photogramm. Remote Sens.*, vol. 58, no. 3–4, pp. 239–258, 2004.

Yuxin Chen is currently working toward the Master's degree in cartography and GIS with the Sichuan Normal University, Chengdu, China.

Weilai Zhang is currently working toward the Master's degree in human geography with the Sichuan Normal University, Chengdu, China, with a research focus on ecosystem services.

Jiajia Yang is currently working toward the Graduate degree in the field of cartography and GIS with the School of Geography and Tourism, Sichuan Normal University, Chengdu, China.

His research interests include remote sensing applications and GIS.

Yuanyuan Xu is currently working toward the Graduate degree in the field of cartography and GIS with the School of Geography and Tourism, Sichuan Normal University, Chengdu, China.

His research interests includes remote sensing applications and GIS.

Qian Yuan is a current working toward the Graduate degree in remote sensing applications with the School of Surveying, Mapping and Land Information Engineering, Henan University of Technology, Zhengzhou, China .

Wuxue Cheng received the M.Sc. degree in forest management from the Northwest Agriculture and Forestry University, Xianyang, China, in July 2007, the Ph.D. degree in physical geography from the Institute of Mountain Hazards and Environment, Chinese Academy of Sciences, Beijing, China, in 2010.

He was a Postdoctoral fellow with Chengdu Institute of Biology from 2013 to 2016. He is currently a Professor with the School of Geography and Resource Science, Sichuan Normal University, Chengdu, China, focusing on ecological remote sensing research.

Li Peng received the M.S. and Ph.D. degrees in physical geography from the University of Chinese Academy of Sciences, Beijing, China, in 2008 and 2013, respectively.

He is currently a Professor with the College of Geography and Resources, Sichuan Normal University. He is the author who published more than 20 SCI/SSCI articles. His research interests include hazard risk assessment and land use planning. He is a reviewer of SCI/SSCI journal, such as IEEE Access, Natural Hazards, the International Journal of Disaster Risk Science, and Land Degradation & Development.